ACS APPLIED OPTICAL MATERIALS

pubs.acs.org/acsaom Article

Facile Optical Gap Tuning in Nanographene Metal–Organic Frameworks

Xin Zheng, Rosmi Reji, Matthew C. Drummer, Haiying He, Jens Niklas, Nicholas P. Weingartz, Igor L. Bolotin, Lin X. Chen, Oleg G. Poluektov, Peter Zapol, and Ksenija D. Glusac*

Cite This: ACS Appl. Opt. Mater. 2023, 1, 1643–1650 Read Online

ACCESS | Metrics & More | Article Recommendations | Supporting Information

ABSTRACT: The utilization of metal–organic frameworks (MOFs) in photocatalysis applications requires light-responsive architectures with tunable optical gaps. Here, we demonstrate a facile approach to optical gap tuning via postsynthetic modifications of pbz-MOF-1, a Zr-based MOF with polyphenylene ligands. A simple reaction of pbz-MOF-1 with $FeCl_3$ was shown to induce three different chemical reactions: oxidative dehydrogenation, chlorination, and one-electron oxidation of the ligands. The result of these reactions was a gradual decrease in the optical gap from 2.95 eV to as little as 0.69 eV. Steady-state and time-resolved optical spectroscopy, mass spectrometry, and electron paramagnetic resonance spectroscopy, coupled with density functional theory calculations, provide insights into the chemical transformations that affect the optical properties of the MOF. The facile optical gap tuning reported here has promising application in the utilization of photoresponsive MOFs in photocatalysis, sensing, and other light-triggered applications.

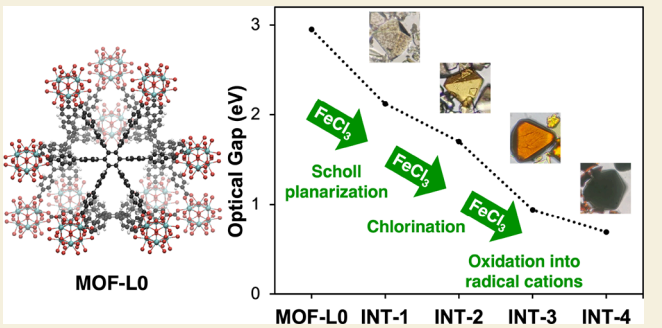

KEYWORDS: *zirconium metal–organic frameworks, postsynthetic modification, optical gap tuning, stable aromatic radical cation, transient absorption spectroscopy*

INTRODUCTION

Light-harvesting metal–organic frameworks (MOFs) have been extensively studied during the past decade.[1−7] These scaffolds were shown to enhance energy transport distances by increasing the excited state lifetime of the chromophore, by improving the electronic coupling between the chromophores or by orienting chromophores' transition dipole moments into the ideal geometry for resonance energy transfer.[1−7] For example, the electronic coupling between chromophore ligands can be readily tuned by changing the MOF topology, leading to exciton coherence lengths that range from one (no electronic coupling) to more than four linkers.[8,9] Furthermore, the rigidification of chromophores within the MOF scaffold was shown to increase the excited state lifetimes of ligands.[10−14] This effect was most drastic when MOFs were constructed from chromophores that are nonemissive due to the existence of nonradiative excited-state decay pathways associated with low-frequency phenyl ring torsions and C=C bond stretches.[10,11] The electronic energy transfer in MOFs was studied for both singlet[15,16] and triplet[17,18] excited states. In general, the exciton diffusivity of singlets ($\sim 10^{-5}$ m^2/s) was found to be higher than that of triplets ($\sim 10^{-10}$ m^2/s), which is consistent with the spin-forbiddenness of long-range resonance energy transfer involving triplet excited states.[5] However, spin–orbit coupling mechanisms can enable singlet resonance energy transfer from triplet-forming chromophores that contain heavy atoms.[19] Furthermore, triplet excited state lifetimes tend to be longer than those of singlet excitons, resulting in high exciton diffusion lengths reported for both types of excited states. Molecular photoswitches can be used to control energy transfer in MOFs.[20,21] Even though the rigidification of a photoswitch inside the MOF significantly reduces the switching rate,[22] efficient photoswitching of energy transfer can be achieved when flexible MOFs are used[23] or when the photoswitch is loosely bound in the MOF pores.[24,25] The photoswitching is usually achieved by controlling the energy transfer from a chromophore to the molecular switch, whose excited-state energies are tuned so that the energy transfer is feasible to one form of the switch and not the other. The control of energy transfer in MOFs was also achieved via anisotropic energy transfer. For example, directional energy transfer was demonstrated in several two-dimensional MOFs by taking advantage of different degrees of electronic coupling

Received: June 24, 2023
Revised: September 8, 2023
Accepted: September 8, 2023
Published: October 16, 2023

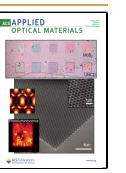

Scheme 1. Illustration of the Progress of the MOF Reaction with $FeCl_3$

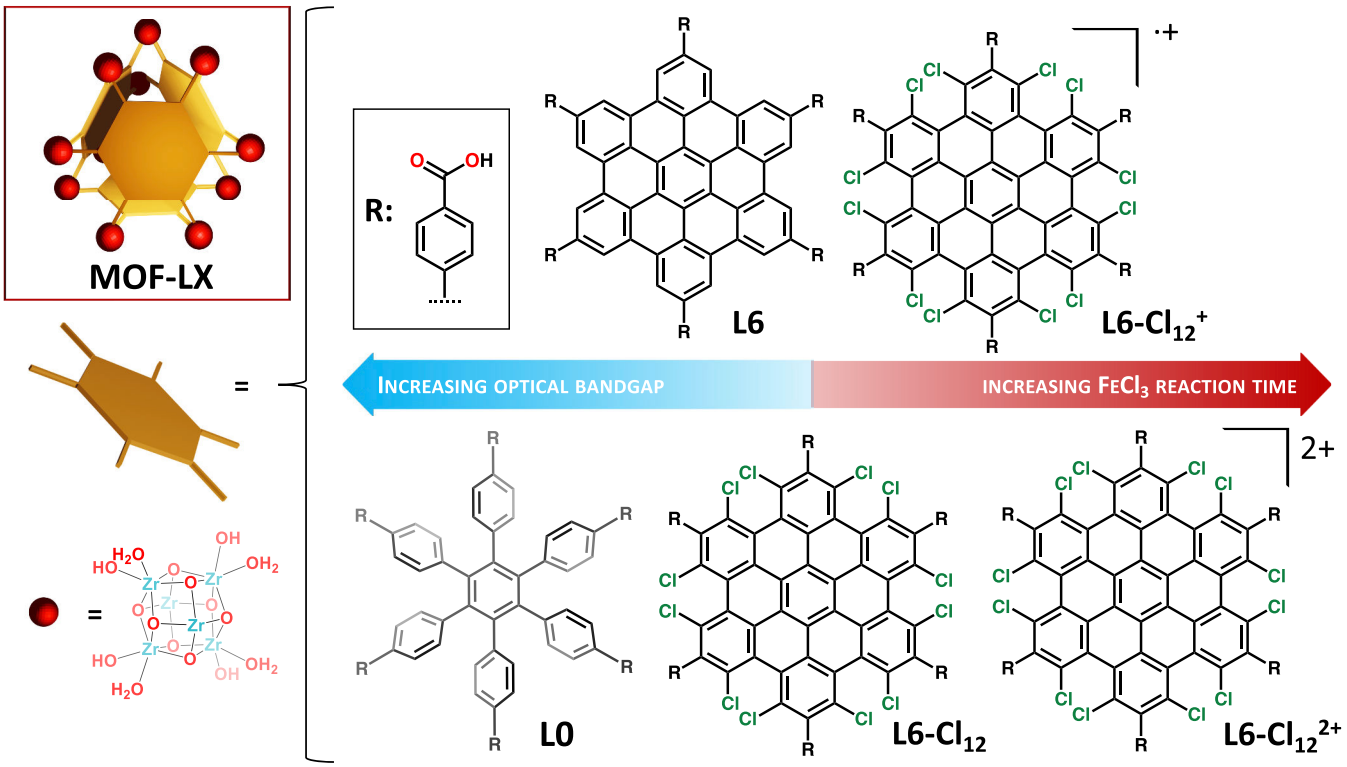

experienced between interlayer and intralayer chromophores.[15,26−28] These energy transfer anisotropy experiments are generally performed using MOFs grown from surfaces using layer-by-layer deposition, where the layer thickness can be readily controlled, and the excited state quenchers can be introduced at controlled positions.

Application of light-responsive MOFs in photocatalysis requires that their optical gaps be readily tuned across the visible spectral range.[1] For example, the valence band potential of MOFs for artificial photosynthesis should be more positive than the standard reduction potential for the oxygen evolution reaction. Similarly, their conduction band potential should be more negative than the standard reduction potential for carbon dioxide reduction. At the same time, the optical gap of the MOF should not exceed 3.2 eV to ensure utilization of the visible part of the solar spectrum.[29] When MOFs are made of optically silent metal ions, such as d^0 Zr^{4+} or d^{10} Zn^{2+} ions, optical gap tuning can be achieved only via chemical modifications of the linker. Many studies have shown that the optical gap narrowing in MOFs can be achieved either by increasing the conjugation length[30−34] or by the introduction of electron-withdrawing or accepting groups to the ligand.[35−37] The chromophore ligands for light-responsive MOFs are usually selected from the class of porphyrin-,[15,38−40] aryl-,[28,41−46] or transition metal-based motifs.[17,47−49] In general, the MOF optical gap shifts were found to correlate well with the changes in the ionization potentials and electron affinities of isolated ligands with different substituents.[50] While ligand modifications provide excellent tunability of MOF optical gaps, the synthesis of ligands with varying conjugation lengths or functional groups is often challenging. To circumvent these challenges, several reports have shown that the optical gap tuning can be achieved via postsynthetic modifications (PSM) of the MOF ligands. This approach often starts with a MOF that contains an amino-functionalized ligand, which is postsynthetically modified using either diazotization reaction[51,52] or condensation with aldehydes[53] to extend the conjugation and decrease the optical gap. Ligand amino groups were also used for incorporation of transition metal ions to achieve enhanced light absorption and optical gap tuning.[54] A type of noncovalent PSM by introducing amine vapor and generating stable radical anions on MOF ligands via photoinduced electron transfer has also been demonstrated to effectively reduce the optical gap and extend light absorption over the entire visible range.[45]

RESULTS AND DISCUSSION

The PSM of polyphenylene-based ligands using oxidative dehydrogenation was shown previously to efficiently tune the optical gap of Zr-based MOFs.[55] Here, we extend these studies by showing that a simple reagent, $FeCl_3$, can be used to additionally modify nanographene ligands to form MOF intermediates (**INT-1**, **INT-2**, **INT-3**, and **INT-4**) with optical gaps that range from 2.12 to 0.69 eVs. Specifically, the reaction between a Zr-based **MOF-L0** (also known as **pbz-MOF-1**[56]) and $FeCl_3$ was shown to generate intermediate MOFs with absorption that red-shifts from 345 to 850 nm. Based on the mechanistic studies in this current report, we assign this red shift to the successive formation of MOFs with planarized ligands (**MOF-L6**, also known as **PCN-136**[55]) and absorption at 490 nm, MOFs with chlorinated and planarized ligands (**MOF-L6-Cl$_n$**) and absorption at 615 nm, and MOFs with oxidized radical cation (and possibly dication) ligands (**MOF-L6-Cl$_n^+$** and **MOF-L6-Cl$_n^{2+}$**) and the lowest-energy absorption band at 800 nm (Scheme 1).

The synthesis of **MOF-L0** (**pbz-MOF-1**) was achieved using the previously reported procedure (details are presented in the SI).[56] Figure 1a illustrates the changes in the UV/vis

https://doi.org/10.1021/acsaom.3c00220
ACS Appl. Opt. Mater. 2023, 1, 1643−1650

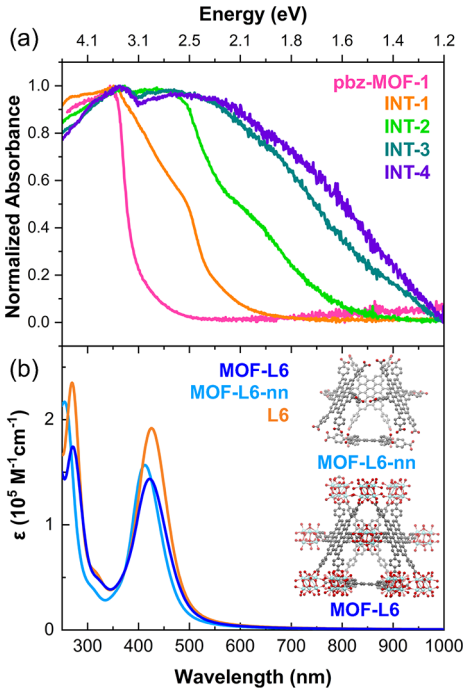

Figure 1. (a) UV/vis diffuse reflectance spectra of MOF intermediates prepared from reactions with $FeCl_3$ in 5:1 v/v nitromethane/dichloromethane solvent with varying reaction times; (b) calculated UV−vis absorption spectra of **MOF-L6**, **MOF-L6-nn** (nn stands for no nodes), and **L6** at the HSE06 level of theory.

reflectance of the MOF samples as the reaction with $FeCl_3$ proceeds (reaction conditions are described in the SI). While the lowest-energy absorption band for the **MOF-L0** precursor appears at 345 nm, it shifts to 490 nm for **INT-1**, 615 nm for **INT-2**, and ∼800 nm for **INT-3** and **INT-4**. A small red-shift is expected when considering the UV−vis absorption spectra of **MOF-L0** to **MOF-L6** in the presence of $FeCl_3$ as an oxidant, as shown in Figure S22. We calculated the UV/vis absorption spectrum of **MOF-L6** at the HSE06 level of theory (Figure 1b). The calculated absorption spectrum consists of three absorption bands with maxima at 238, 271, and 422 nm. The calculated 422 nm absorption band is in good agreement with the experimentally observed 490 nm band in intermediate samples **INT-1** to **INT-4**, so we assign this absorption feature to the **L6** ligand moieties of the MOF samples. Importantly, the calculated spectrum does not predict any absorption beyond 600 nm, indicating that **MOF-L6** is not responsible for the experimentally observed UV/vis absorption in the red region of the visible spectrum.

The calculations were extended to explore the contribution of Zr-nodes to the electronic transitions by investigating the UV/vis absorption spectrum of the MOF in the absence of nodes, where ligand carboxylates are terminated with protons to form −COOH groups (**MOF-L6-nn**, where nn stands for no nodes, Figure 1b). The lowest-energy bands at ∼420 nm for **MOF-L6-nn** and **MOF-L6** are almost identical, confirming the ligand-centered π,π^* electronic transitions. The Zr-nodes do not contribute to the absorption at 420 nm. Instead, the nodes contribute to the UV peak at 270 nm in the form of O $2p \rightarrow$ Zr $4d$ electronic transitions.[57,58] We also find that the calculated absorption spectra of ligands arranged in the same geometry as they adopt in the framework (**MOF-L6-nn**) are quite similar to that of the isolated ligand **L6**. Only a slight blue shift was observed for **MOF-L6-nn** relative to **L6**, indicating minimal electronic communication between the ligands. This result is consistent with the relatively large spacing between ligands inside **MOF-L6**: the center-to-center distance between adjacent chromophore ligands is 15.8 Å, and the acute dihedral angle between the planes defined by adjacent **L6** ligands is 70.5°. Similar observations of weak interligand electronic coupling reported in other Zr-based MOFs illustrate that these frameworks consist of collections of isolated ligand chromophores.[8] Furthermore, a previously reported MOF made from hexabenzocoronene-containing ligands similar to **L6** was shown to be yellow in color,[59] supporting our conclusions that **MOF-L6** absorbs in the blue part of the visible spectrum.

To obtain further insight into the chemical transformations taking place during the reaction with $FeCl_3$, intermediate MOF samples were studied using mass spectrometry (MS, details are provided in the SI). The mass spectra of digested ligands of intermediate MOFs, along with the simulated spectra for the relevant species, are shown in Figures 2a−d and illustrate the heterogeneity of the samples. The MS of **INT-1** is relatively simple and indicates the presence of **L0** ligand (its methyl esterified "ME" and sulfonated "SO_3H" derivatives are expected to form during digestion and sample preparation in H_2SO_4/CH_3OH) and monochlorinated **L0-Cl$_1$** derivative. Interestingly, the presence of **L6** was not confirmed in the MS data, even though the UV/vis reflectance spectrum of **INT-1** (Figure 1) indicates that **L0**-to-**L6** conversion likely took place, at least to some degree. We postulate that the absence of **L6** peaks in our MS data is due to the low solubility of **L6**. Based on these results, we conclude that **INT-1** is a mixed-ligand MOF composed of **L0** and **L6** moieties. The digested **INT-2**, **INT-3**, and **INT-4** samples exhibit MS peaks consistent with the unreacted **L0** derivative as well as the chlorinated **L6-Cl$_n$** ligands. The degree of chlorination, and thus the value of n in **L6-Cl$_n$**, increases from **INT-2** to **INT-3** to **INT-4**, indicating that the reaction with $FeCl_3$ involves the initial conversion of **L0** to **L6**, followed by the chlorination of **L6** hexabenzocoronene edges, to generate **L6-Cl$_n$** ligands, where n ranges from 1 to 12. Again, we hypothesize that **INT-2**, **INT-3**, and **INT-4** contain **L6** but that this ligand is not detectable in MS due to low solubility. The presence of chlorinated ligand is consistent with a previous report showing that $FeCl_3$ effectively planarizes and chlorinates nanographenes in a one-step reaction under solvent-free conditions.[60]

The MOF samples were also investigated using electron paramagnetic resonance (EPR) spectroscopy (Figure 3), which revealed that all intermediate MOFs contain a signal at $g \approx 2.003-2.004$. This signal does not demonstrate any resolved hyperfine structure, which is indicative of organic radical with highly delocalized electron spin density. The area of this radical signal increases more than 40 times going from **INT-2** to **INT-4** (this value is a qualitative estimate obtained under an assumption that **INT-2** and **INT-4** measurements were obtained with the equal amounts of the sample). Based on these findings, we conclude that the reaction of **MOF-L0** with $FeCl_3$ involves three different processes: (i) oxidative dehydrogenation of **MOF-L0** to form **MOF-L6**; (ii) chlorination of **MOF-L6** to form **MOF-L6-Cl$_n$** (n = 3−12); (iii) oxidation of **MOF-L6-Cl$_n$** to form one-electron oxidized **MOF-L6-Cl$_n^{\bullet+}$**.

The evaluation of the contribution that each ligand moiety makes in the overall absorption spectrum of MOF samples was

https://doi.org/10.1021/acsaom.3c00220
ACS Appl. Opt. Mater. 2023, 1, 1643−1650

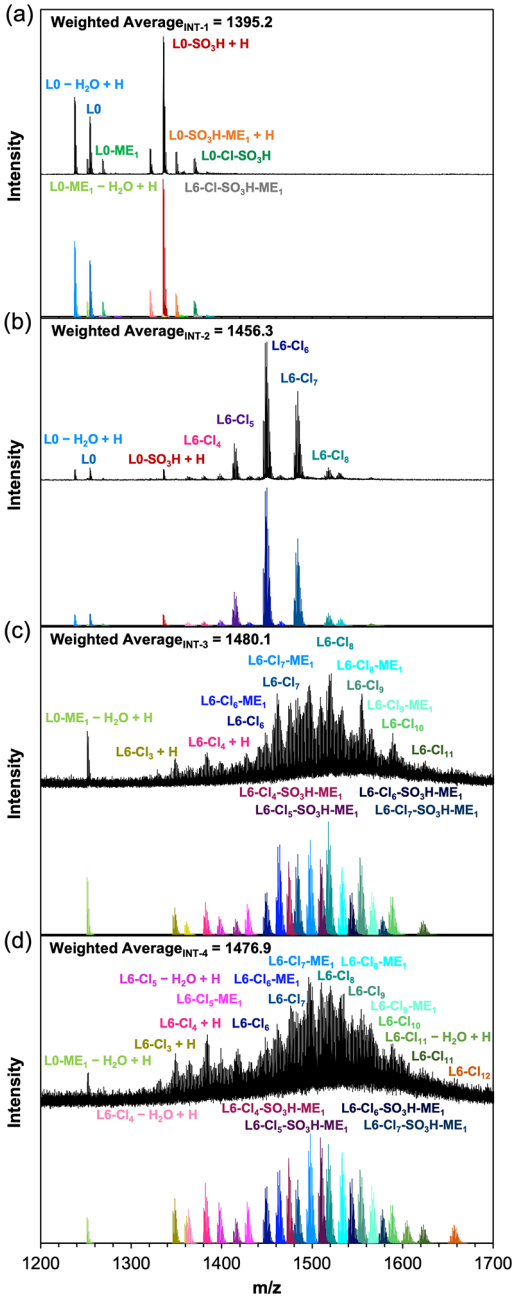

Figure 2. Experimental (top) and simulated (bottom) mass spectra of ligands obtained upon the digestion of (a) **INT-1**, (b) **INT-2**, (c) **INT-3**, and (d) **INT-4**. The simulated profiles were generated using *EnviPat*.[61] The weighted average is calculated based on data in the m/z = 1200−1700 range. Full peak assignment is given in the SI.

achieved by independently synthesizing the relevant ligands **L0**, **L6**, **L6-Cl$_{12}$**, and **L6-Cl$_{12}^{+}$** (synthesis and characterization details are presented in the SI). The experimental absorption spectra of these ligands are shown in Figure 4, along with the calculated spectra obtained at the HSE06 level of theory. The peak in the experimental absorption spectrum of **L0** appears at 293 nm, which is in excellent agreement with the calculated absorption wavelength of 289 nm. The experimental lowest-energy absorption band of planarized **L6** appears at 377 nm (calculated value is at 428 nm), while the absorption spectrum of **L6-Cl$_{12}$** is slightly red-shifted relative to **L6** and exhibits the lowest energy band at 406 (experiment) and 458 nm

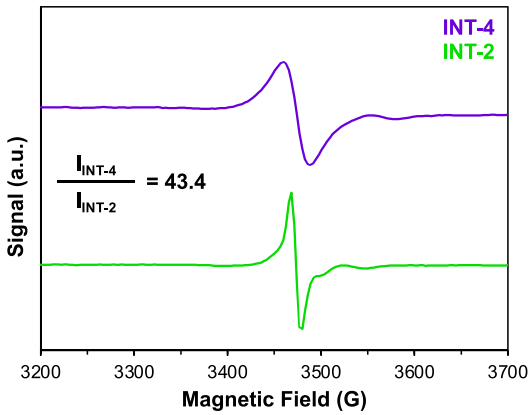

Figure 3. EPR spectra of **INT-2** and **INT-4**. The ratio of the peak integrals is 43.4, where the double integrals I_{INT-2} and I_{INT-4} are estimated using (peak-to-trough amplitude) × (linewidth)^2.

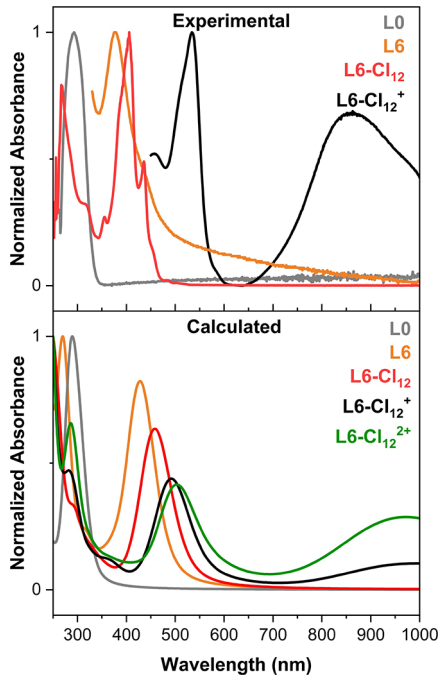

Figure 4. Top: experimental UV−vis absorption spectra of **L0** in DMF, **L6** in aqueous 1 wt % SDBS, **L6-Cl$_{12}$** in DMF, and **L6-Cl$_{12}^{+}$** in $SbCl_5$. Bottom: calculated UV−vis absorption spectra of ligands at the HSE06 level of theory.

(calculation). These absorption bands are in reasonable agreement with the ∼470 nm shoulder observed in **INT-1** (the same absorption band is also present in the UV-Vis reflectance spectra of **INT-2**, **INT-3**, and **INT-4**) and are consistent with observed presence of chlorinated and planarized ligands in the MS data of **INT-2**, **INT-3**, and **INT-4** (Figure 2). Finally, the experimental absorption spectrum of radical cation **L6-Cl$_{12}^{+}$** consists of the visible band at 534 nm and a broad shoulder in the near-IR region, with a maximum at 863 nm and is qualitatively similar to the calculated spectrum of **L6-Cl$_{12}^{+}$**. The 534 nm band is in reasonable agreement with the 615 nm shoulder observed in **INT-2** (this absorption band is also present in **INT-3** and **INT-4**). Thus, we hypothesize that the experimentally observed MOF absorption features that extend into the near-IR region in Figure 1 are likely associated with the presence of

https://doi.org/10.1021/acsaom.3c00220
ACS Appl. Opt. Mater. 2023, 1, 1643−1650

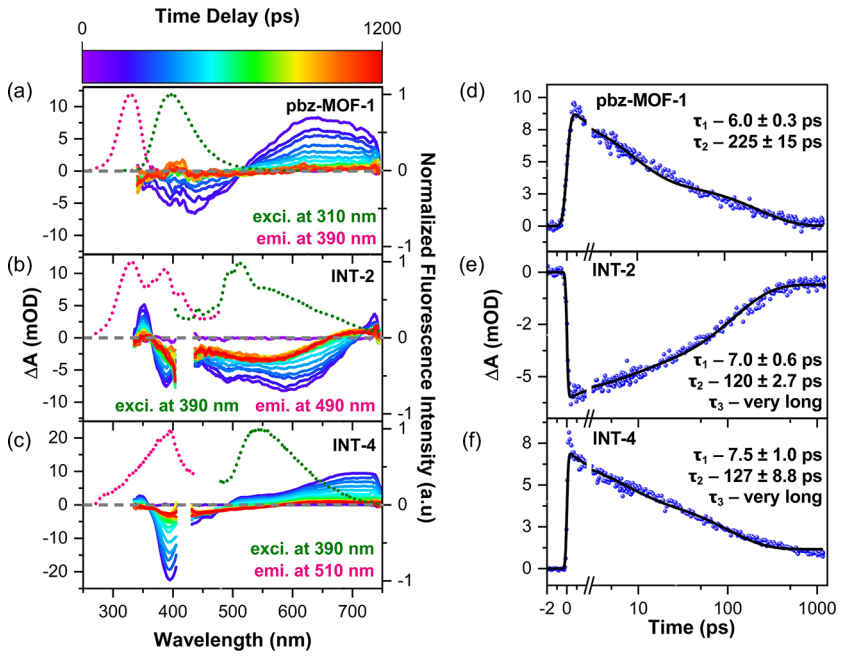

Figure 5. Femtosecond transient absorption spectra for MOF intermediates. (a–c) Spectral trace for **pbz-MOF-1** (ex −315 nm), **INT-2** (ex −410 nm), and **INT-4** (ex −410 nm) in DMF suspension. Transient spectra were collected in time intervals ranging from 0 to 1200 ps. Dotted lines present the fluorescence excitation (pink) and emission (green) spectra for each MOF intermediate suspended in DMF. Emission spectra were collected upon excitation at 390 nm, while excitation spectra were collected by monitoring the emission at 490 nm. (d–f) Kinetic traces for MOF intermediates monitored at 650 nm. Solid black lines show fits for the sequential kinetic model. Lifetime for each component present in each MOF intermediate is given.

L6^{+} and **L6-Cl**$_n^{+}$ radical cation moieties. This assignment is consistent with the EPR signals observed for intermediate MOFs (Figure 3 and Figure S18). Furthermore, there are literature precedents of stable aromatic radical cations generated in the presence of $FeCl_3$ and $SbCl_5$ under ambient conditions.[62−66] Interestingly, our calculations indicate that the absorption spectra of the **L6-Cl**$_{12}^{+}$ radical cation and that of the **L6-Cl**$_{12}^{2+}$ dication are similar, making it possible that the MOF intermediates also contain dication moieties. However, we were unable to experimentally confirm the presence of dication species in our MOF intermediates.

The changes in the emission and excitation spectra of MOF intermediates are shown as dotted lines in Figure 5. The prolonged reaction with $FeCl_3$ causes the red shift of the emission band from 394 nm in **MOF-L0** to 545 nm in **INT-4**. Similarly, the excitation spectra shift from 330 to 396 nm, and this shift is consistent with the observed changes in the UV/vis absorption spectra going from **L0** to **L6** and **L6-Cl**$_{12}$ (Figure 4). Thus, we assign the emission observed in Figure 5 to the fluorescence from singlet excited states of MOFs that contain a mixture of **L0**, **L6**, and **L6-Cl**$_n$ ligands. As the reaction time with $FeCl_3$ increases, we observe a loss of emission due to **L0** moieties and an increase in the emission from **L6** and **L6-Cl**$_n$ ligands. The lifetimes of these species were determined by femtosecond transient absorption spectroscopy (Figure 5 and Figure S25). All MOF intermediates were found to exhibit two main transient components with lifetimes of τ_1 = 6.0−10 ps and τ_2 = 120−225 ps. The τ_1 component is assigned to the vibrational relaxation from ligand-centered vibrationally "hot" S_1 states of the MOFs, while the τ_2 process is assigned to the $S_1 \rightarrow S_0$ conversion. This assignment is consistent with the loss of the stimulated emission signal at 400 nm for **pbz-MOF-1**, as well as the loss of the ground-state bleach signal at 400 nm for **INT-2** and **INT-4**. Based on this assignment, the excited states localized on **L0**, **L6**, and **L6-Cl**$_n$ ligand moieties are relatively short-lived, in the 120−226 ps range. It is interesting to note that **INT-2**, **INT-3**, and **INT-4** exhibit an additional long-lived component with ground-state bleach that extends throughout the visible range up to 700 nm. This long-lived transient was explored using nanosecond transient absorption (Figure S26), and the kinetics were found to be biexponential with lifetimes of τ_3 = 0.5−1.2 μs and τ_2 = 9−14 μs. Based on our previous time-resolved EPR study,[67] we assign these transients to the ligand-centered T_1 and radical cation states. Since the ground-state bleach of these transients extends beyond 500 nm, they are not associated with **L0**, **L6** or **L6-Cl**$_n$ ligand moieties. Instead, we assign these transients to the radical cation or dication species. Given the high degree of heterogeneity of our samples, it is not possible to make a more detailed assignment of the transients. However, it is important to mention that the long-lived transients arise from radical cation and dication moieties of the MOF, indicating that these may be important moieties in photocatalytic applications.[67]

CONCLUSIONS

In summary, we report a simple chemical method to tune the optical gap of MOFs using $FeCl_3$ as an oxidant. We demonstrate that the reaction of **MOF-L0** with $FeCl_3$ involves the conversion of **L0** ligands to **L6**, **L6-Cl**$_n$, and **L6-Cl**$_n^{+}$ species, resulting in the optical gap reduction from 2.95 to 0.69 eV (Scheme 2). This work is anticipated to have an impact on utilization of MOFs in light-driven processes, such as sensing and photocatalysis. Because 43% of the solar energy reaching the surface of Earth is in the 400−700 nm visible light range and only 4% of the solar energy is in the <400 nm region,[68] the optical gap tuning of MOF photocatalysts extending light absorption into longer-wavelength regions can increase the

https://doi.org/10.1021/acsaom.3c00220
ACS Appl. Opt. Mater. 2023, 1, 1643−1650

Scheme 2. Experimental and Calculated Lowest-Energy Transition Energies for L0, L6, L6-Cl_{12}, L6-Cl_{12}^{+}, and L6-Cl_{12}^{2+}[a]

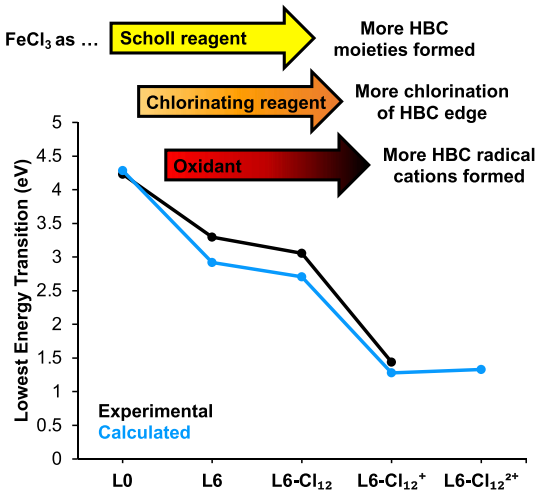

[a]HBC: hexa-*peri*-hexabenzocoronene.

solar-to-fuel conversion efficiency in reactions such as CO_2 reduction[55,67,69] and H_2 evolution.[54,68,70] In addition to improving light harvesting, the fine-tuning of the optical band edges also enables precise optical gap edge straddling of the redox potentials of the reaction of interest and can potentially improve selectivity of the photoreaction.[1,29,50]

■ ASSOCIATED CONTENT

Supporting Information

The Supporting Information is available free of charge at https://pubs.acs.org/doi/10.1021/acsaom.3c00220.

Ligands and MOFs syntheses and characterizations and computational methods (PDF)

■ AUTHOR INFORMATION

Corresponding Author

Ksenija D. Glusac − *Department of Chemistry, University of Illinois Chicago, Chicago, Illinois 60607, United States; Chemical Sciences and Engineering Division, Argonne National Laboratory, Lemont, Illinois 60439, United States;* orcid.org/0000-0002-2734-057X; Email: glusac@uic.edu

Authors

Xin Zheng − *Department of Chemistry, University of Illinois Chicago, Chicago, Illinois 60607, United States;* orcid.org/0000-0002-5506-8112

Rosmi Reji − *Department of Chemistry, University of Illinois Chicago, Chicago, Illinois 60607, United States; Chemical Sciences and Engineering Division, Argonne National Laboratory, Lemont, Illinois 60439, United States*

Matthew C. Drummer − *Department of Chemistry, University of Illinois Chicago, Chicago, Illinois 60607, United States; Chemical Sciences and Engineering Division, Argonne National Laboratory, Lemont, Illinois 60439, United States*

Haiying He − *Department of Physics and Astronomy, Valparaiso University, Indiana 46383, United States*

Jens Niklas − *Chemical Sciences and Engineering Division, Argonne National Laboratory, Lemont, Illinois 60439, United States;* orcid.org/0000-0002-6462-2680

Nicholas P. Weingartz − *Chemical Sciences and Engineering Division, Argonne National Laboratory, Lemont, Illinois 60439, United States; Department of Chemistry, Northwestern University, Evanston, Illinois 60208, United States*

Igor L. Bolotin − *Department of Chemistry, University of Illinois Chicago, Chicago, Illinois 60607, United States*

Lin X. Chen − *Chemical Sciences and Engineering Division, Argonne National Laboratory, Lemont, Illinois 60439, United States; Department of Chemistry, Northwestern University, Evanston, Illinois 60208, United States*

Oleg G. Poluektov − *Chemical Sciences and Engineering Division, Argonne National Laboratory, Lemont, Illinois 60439, United States;* orcid.org/0000-0003-3067-9272

Peter Zapol − *Materials Science Division, Argonne National Laboratory, Lemont, Illinois 60439, United States;* orcid.org/0000-0003-0570-9169

Complete contact information is available at: https://pubs.acs.org/10.1021/acsaom.3c00220

Funding

This work is supported by the U.S. Department of Energy (DOE), Office of Science, Office of Basic Energy Science, Division of Chemical Sciences, Geosciences, and Biosciences, through Argonne National Laboratory under Contract No. DE-AC02−06CH11357.

Notes

The authors declare no competing financial interest.

■ ACKNOWLEDGMENTS

We thank Daniel J. McElheny for EPR simulation and helpful suggestions. We also thank Sreenivasulu Chinnabattigalla and Juan P. Vizuet for their useful advice.

■ ABBREVIATIONS

MOF, metal−organic framework; DMF, *N*,*N*-dimethylformamide; SDBS, sodium dodecylbenzenesulfonate; HBC, hexa-*peri*-hexabenzocoronene.

■ REFERENCES

(1) Guo, X.; Liu, L.; Xiao, Y.; Qi, Y.; Duan, C.; Zhang, F. Band gap engineering of metal-organic frameworks for solar fuel productions. *Coord. Chem. Rev.* **2021**, *435*, No. 213785.

(2) Pattengale, B.; Ostresh, S.; Schmuttenmaer, C. A.; Neu, J. Interrogating Light-initiated Dynamics in Metal-Organic Frameworks with Time-resolved Spectroscopy. *Chem. Rev.* **2022**, *122* (1), 132−166.

(3) So, M. C.; Wiederrecht, G. P.; Mondloch, J. E.; Hupp, J. T.; Farha, O. K. Metal-organic framework materials for light-harvesting and energy transfer. *Chem. Commun.* **2015**, *51* (17), 3501−3510.

(4) Wang, J. L.; Wang, C.; Lin, W. Metal-Organic Frameworks for Light Harvesting and Photocatalysis. *ACS Catal.* **2012**, *2* (12), 2630−2640.

(5) Wang, Z.; Wang, C. Excited State Energy Transfer in Metal-Organic Frameworks. *Adv. Mater.* **2021**, *33* (50), No. 2005819.

(6) Yu, J.; Li, X.; Deria, P. Light-Harvesting in Porous Crystalline Compositions: Where We Stand toward Robust Metal-Organic Frameworks. *ACS Sustainable Chem. Eng.* **2019**, *7* (2), 1841−1854.

(7) Zhang, T.; Lin, W. Metal-organic frameworks for artificial photosynthesis and photocatalysis. *Chem. Soc. Rev.* **2014**, *43* (16), 5982−5993.
(8) Deria, P.; Yu, J.; Balaraman, R. P.; Mashni, J.; White, S. N. Topology-dependent emissive properties of zirconium-based porphyrin MOFs. *Chem. Commun.* **2016**, *52* (88), 13031−13034.
(9) Yu, J.; Park, J.; Van Wyk, A.; Rumbles, G.; Deria, P. Excited-State Electronic Properties in Zr-Based Metal-Organic Frameworks as a Function of a Topological Network. *J. Am. Chem. Soc.* **2018**, *140* (33), 10488−10496.
(10) Shustova, N. B.; McCarthy, B. D.; Dinca, M. Turn-On Fluorescence in Tetraphenylethylene-Based Metal-Organic Frameworks: An Alternative to Aggregation-Induced Emission. *J. Am. Chem. Soc.* **2011**, *133* (50), 20126−20129.
(11) Shustova, N. B.; Cozzolino, A. F.; Dinca, M. Conformational Locking by Design: Relating Strain Energy with Luminescence and Stability in Rigid Metal-Organic Frameworks. *J. Am. Chem. Soc.* **2012**, *134* (48), 19596−19599.
(12) Wei, Z.; Gu, Z. Y.; Arvapally, R. K.; Chen, Y. P.; McDougald, R. N.; Ivy, J. F.; Yakovenko, A. A.; Feng, D.; Omary, M. A.; Zhou, H. C. Rigidifying Fluorescent Linkers by Metal-Organic Framework Formation for Fluorescence Blue Shift and Quantum Yield Enhancement. *J. Am. Chem. Soc.* **2014**, *136* (23), 8269−8276.
(13) Yin, H. Q.; Wang, X. Y.; Yin, X. B. Rotation Restricted Emission and Antenna Effect in Single Metal-Organic Frameworks. *J. Am. Chem. Soc.* **2019**, *141* (38), 15166−15173.
(14) Liu, Y. Y.; Zhang, X.; Li, K.; Peng, Q. C.; Qin, Y. J.; Hou, H. W.; Zang, S. Q.; Tang, B. Z. Restriction of Intramolecular Vibration in Aggregation-Induced Emission Luminogens: Applications in Multifunctional Luminescent Metal-Organic Frameworks. *Angew. Chem., Int. Ed.* **2021**, *60* (41), 22417−22423.
(15) Son, H. J.; Jin, S. Y.; Patwardhan, S.; Wezenberg, S. J.; Jeong, N. C.; So, M.; Wilmer, C. E.; Sarjeant, A. A.; Schatz, G. C.; Snurr, R. Q.; Farha, O. K.; Wiederrecht, G. P.; Hupp, J. T. Light-Harvesting and Ultrafast Energy Migration in Porphyrin-Based Metal-Organic Frameworks. *J. Am. Chem. Soc.* **2013**, *135* (2), 862−869.
(16) Lee, C. Y.; Farha, O. K.; Hong, B. J.; Sarjeant, A. A.; Nguyen, S. T.; Hupp, J. T. Light-Harvesting Metal-Organic Frameworks (MOFs): Efficient Strut-to-Strut Energy Transfer in Bodipy and Porphyrin-Based MOFs. *J. Am. Chem. Soc.* **2011**, *133* (40), 15858−15861.
(17) Kent, C. A.; Mehl, B. P.; Ma, L.; Papanikolas, J. M.; Meyer, T. J.; Lin, W. Energy Transfer Dynamics in Metal-Organic Frameworks. *J. Am. Chem. Soc.* **2010**, *132* (37), 12767−12769.
(18) Maza, W. A.; Padilla, R.; Morris, A. J. Concentration Dependent Dimensionality of Resonance Energy Transfer in a Postsynthetically Doped Morphologically Homologous Analogue of UiO-67 MOF with a Ruthenium(II) Polypyridyl Complex. *J. Am. Chem. Soc.* **2015**, *137* (25), 8161−8168.
(19) Chakraborty, A.; Ilic, S.; Cai, M.; Gibbons, B. J.; Yang, X.; Slamowitz, C. C.; Morris, A. J. Role of Spin-Orbit Coupling in Long Range Energy Transfer in Metal-Organic Frameworks. *J. Am. Chem. Soc.* **2020**, *142* (48), 20434−20443.
(20) Rice, A. M.; Martin, C. R.; Galitskiy, V. A.; Berseneva, A. A.; Leith, G. A.; Shustova, N. B. Photophysics Modulation in Photoswitchable Metal-Organic Frameworks. *Chem. Rev.* **2020**, *120* (16), 8790−8813.
(21) Bigdeli, F.; Lollar, C. T.; Morsali, A.; Zhou, H. Switching in Metal-Organic Frameworks. *Angew. Chem., Int. Ed.* **2020**, *59* (12), 4652−4669.
(22) Williams, D. E.; Martin, C. R.; Dolgopolova, E. A.; Swifton, A.; Godfrey, D. C.; Ejegbavwo, O. A.; Pellechia, P. J.; Smith, M. D.; Shustova, N. B. Flipping the Switch: Fast Photoisomerization in a Confined Environment. *J. Am. Chem. Soc.* **2018**, *140* (24), 7611−7622.
(23) Williams, D. E.; Rietman, J. A.; Maier, J. M.; Tan, R.; Greytak, A. B.; Smith, M. D.; Krause, J. A.; Shustova, N. B. Energy Transfer on Demand: Photoswitch-Directed Behavior of Metal-Porphyrin Frameworks. *J. Am. Chem. Soc.* **2014**, *136* (34), 11886−11889.
(24) Park, J.; Jiang, Q.; Feng, D.; Zhou, H. Controlled Generation of Singlet Oxygen in Living Cells with Tunable Ratios of the Photochromic Switch in Metal-Organic Frameworks. *Angew. Chem.* **2016**, *55* (25), 7188−7193.
(25) Zhao, T.; Han, J.; Shi, Y.; Zhou, J.; Duan, P. Multi-Light-Responsive Upconversion-and-Downshifting-Based Circularly Polarized Luminescent Switches in Chiral Metal-Organic Frameworks. *Adv. Mater.* **2021**, *33* (33), No. 2101797.
(26) Goswami, S.; Ma, L.; Martinson, A. B. F.; Wasielewski, M. R.; Farha, O. K.; Hupp, J. T. Toward Metal Organic Framework-Based Solar Cells: Enhancing Directional Exciton Transport by Collapsing Three-Dimensional Film Structures. *ACS Appl. Mater. Interfaces* **2016**, *8* (45), 30863−30870.
(27) Goswami, S.; Chen, M.; Wasielewski, M. R.; Farha, O. K.; Hupp, J. T. Boosting Transport Distances for Molecular Excitons within Photoexcited Metal-Organic Framework Films. *ACS Appl. Mater. Interfaces* **2018**, *10* (40), 34409−34417.
(28) Haldar, R.; Jakoby, M.; Mazel, A.; Zhang, Q.; Welle, A.; Mohamed, T.; Krolla, P.; Wenzel, W.; Diring, S.; Odobel, F.; Richards, B. S.; Howard, I. A.; Woll, C. Anisotropic energy transfer in crystalline chromophore assemblies. *Nat. Commun.* **2018**, *9*, 4332.
(29) Zhang, T.; Jin, Y.; Shi, Y.; Li, M.; Li, J.; Duan, C. Modulating photoelectronic performance of metal-organic frameworks for premium photocatalysis. *Coord. Chem. Rev.* **2019**, *380*, 201−229.
(30) Lin, C. K.; Zhao, D.; Gao, W. Y.; Yang, Z.; Ye, J.; Xu, T.; Ge, Q.; Ma, S.; Liu, D. J. Tunability of Band Gaps in Metal-Organic Frameworks. *Inorg. Chem.* **2012**, *51* (16), 9039−9044.
(31) Nguyen, H. L.; Vu, T. T.; Le, D.; Doan, T. L. H.; Nguyen, V. Q.; Phan, N. T. S. A Titanium-Organic Framework: Engineering of the Band-Gap Energy for Photocatalytic Property Enhancement. *ACS Catal.* **2017**, *7* (1), 338−342.
(32) Zeng, J. Y.; Wang, X. S.; Xie, B. R.; Li, Q. R.; Zhang, X. Z. Large pi-Conjugated Metal-Organic Frameworks for Infrared-Light-Driven CO2 Reduction. *J. Am. Chem. Soc.* **2022**, *144* (3), 1218−1231.
(33) Nguyen, H. L.; Gandara, F.; Furukawa, H.; Doan, T. L. H.; Cordova, K. E.; Yaghi, O. M. A Titanium-Organic Framework as an Exemplar of Combining the Chemistry of Metal- and Covalent-Organic Frameworks. *J. Am. Chem. Soc.* **2016**, *138* (13), 4330−4333.
(34) Foster, M. E.; Azoulay, J. D.; Wong, B. M.; Allendorf, M. D. Novel metal-organic framework linkers for light harvesting applications. *Chem. Sci.* **2014**, *5* (5), 2081−2090.
(35) Hendon, C. H.; Tiana, D.; Fontecave, M.; Sanchez, C.; D'arras, L.; Sassoye, C.; Rozes, L.; Mellot-Draznieks, C.; Walsh, A. Engineering the Optical Response of the Titanium-MIL-125 Metal-Organic Framework through Ligand Functionalization. *J. Am. Chem. Soc.* **2013**, *135* (30), 10942−10945.
(36) Flage-Larsen, E.; Royset, A.; Cavka, J. H.; Thorshaug, K. Band Gap Modulations in UiO Metal-Organic Frameworks. *J. Phys. Chem. C* **2013**, *117* (40), 20610−20616.
(37) Grau-Crespo, R.; Aziz, A.; Collins, A. W.; Crespo-Otero, R.; Hernandez, N. C.; Rodriguez-Albelo, L. M.; Ruiz-Salvador, A. R.; Calero, S.; Hamad, S. Modelling a Linker Mix-and-Match Approach for Controlling the Optical Excitation Gaps and Band Alignment of Zeolitic Imidazolate Frameworks. *Angew. Chem.* **2016**, *55* (52), 16012−16016.
(38) Fateeva, A.; Chater, P. A.; Ireland, C. P.; Tahir, A. A.; Khimyak, Y. Z.; Wiper, P. V.; Darwent, J. R.; Rosseinsky, M. J. A Water-Stable Porphyrin-Based Metal-Organic Framework Active for Visible-Light Photocatalysis. *Angew. Chem.* **2012**, *51* (30), 7440−7444.
(39) Johnson, J. A.; Luo, J.; Zhang, X.; Chen, Y. S.; Morton, M. D.; Echeverria, E.; Torres, F. E.; Zhang, J. Porphyrin-Metalation-Mediated Tuning of Photoredox Catalytic Properties in Metal-Organic Frameworks. *ACS Catal.* **2015**, *5* (9), 5283−5291.
(40) Zhang, X.; Wasson, M. C.; Shayan, M.; Berdichevsky, E. K.; Ricardo-Noordberg, J.; Singh, Z.; Papazyan, E. K.; Castro, A. J.; Marino, P.; Ajoyan, Z.; Chen, Z.; Islamoglu, T.; Howarth, A. J.; Liu, Y.; Majewski, M. B.; Katz, M. J.; Mondloch, J. E.; Farha, O. K. A historical perspective on porphyrin-based metal-organic frameworks and their applications. *Coord. Chem. Rev.* **2021**, *429*, No. 213615.

https://doi.org/10.1021/acsaom.3c00220
ACS Appl. Opt. Mater. 2023, 1, 1643−1650

(41) Goswami, S.; Yu, J.; Patwardhan, S.; Deria, P.; Hupp, J. T. Light-Harvesting ″Antenna″ Behavior in NU-1000. *ACS Energy Lett.* **2021**, *6* (3), 848−853.
(42) Haldar, R.; Heinke, L.; Woll, C. Advanced Photoresponsive Materials Using the Metal-Organic Framework Approach. *Adv. Mater.* **2020**, *32* (20), No. 1905227.
(43) Kinik, F. P.; Ortega-Guerrero, A.; Ongari, D.; Ireland, C. P.; Smit, B. Pyrene-based metal organic frameworks: from synthesis to applications. *Chem. Soc. Rev.* **2021**, *50* (5), 3143−3177.
(44) Li, X. L.; Yu, J. R.; Gosztola, D. J.; Fry, H. C.; Deria, P. Wavelength-Dependent Energy and Charge Transfer in MOF: A Step toward Artificial Porous Light-Harvesting System. *J. Am. Chem. Soc.* **2019**, *141* (42), 16849−16857.
(45) Lu, B. Z.; Chen, Y. F.; Li, P. Y.; Wang, B.; Mullen, K.; Yin, M. Z. Stable radical anions generated from a porous perylenediimide metal-organic framework for boosting near-infrared photothermal conversion. *Nat. Commun.* **2019**, *10*, 767.
(46) Zhou, Y.; Han, L. Recent advances in naphthalenediimide-based metal-organic frameworks: Structures and applications. *Coord. Chem. Rev.* **2021**, *430*, No. 213665.
(47) Lan, G.; Fan, Y.; Shi, W.; You, E.; Veroneau, S. S.; Lin, W. Biomimetic active sites on monolayered metal-organic frameworks for artificial photosynthesis. *Nat. Catal.* **2022**, *5* (11), 1006−1018.
(48) Lee, Y.; Kim, S.; Fei, H. H.; Kang, J. K.; Cohen, S. M. Photocatalytic CO2 reduction using visible light by metal-monocatecholato species in a metal-organic framework. *Chem. Commun.* **2015**, *51* (92), 16549−16552.
(49) Zhu, J.; Maza, W. A.; Morris, A. J. Light harvesting and energy transfer in ruthenium(II) polypyridyl doped zirconium(IV) metal organic frameworks: A look toward solar cell applications. *J. Photochem. Photobiol., A* **2017**, *344*, 64−77.
(50) Syzgantseva, M. A.; Stepanov, N. F.; Syzgantseva, O. A. Band Alignment as the Method for Modifying Electronic Structure of Metal-Organic Frameworks. *ACS Appl. Mater. Interfaces* **2020**, *12* (15), 17611−17619.
(51) Nasalevich, M. A.; Goesten, M. G.; Savenije, T. J.; Kapteijn, F.; Gascon, J. Enhancing optical absorption of metal-organic frameworks for improved visible light photocatalysis. *Chem. Commun.* **2013**, *49* (90), 10575−10577.
(52) Otal, E. H.; Kim, M. L.; Calvo, M. E.; Karvonen, L.; Fabregas, I. O.; Sierra, C. A.; Hinestroza, J. P. A panchromatic modification of the light absorption spectra of metal-organic frameworks. *Chem. Commun.* **2016**, *52* (40), 6665−6668.
(53) Wei, Y. P.; Liu, Y.; Guo, F.; Dao, X. Y.; Sun, W. Y. Different functional group modified zirconium frameworks for the photocatalytic reduction of carbon dioxide. *Dalton Trans.* **2019**, *48* (23), 8221−8226.
(54) Karthik, P.; Shaheer, A. R. M.; Vinu, A.; Neppolian, B. Amine Functionalized Metal-Organic Framework Coordinated with Transition Metal Ions: d-d Transition Enhanced Optical Absorption and Role of Transition Metal Sites on Solar Light Driven H-2 Production. *Small* **2020**, *16* (12), No. 1902990.
(55) Qin, J. S.; Yuan, S.; Zhang, L.; Li, B.; Du, D. Y.; Huang, N.; Guan, W.; Drake, H. F.; Pang, J.; Lan, Y. Q.; Alsalme, A.; Zhou, H. C. Creating Well-Defined Hexabenzocoronene in Zirconium Metal-Organic Framework by Postsynthetic Annulation. *J. Am. Chem. Soc.* **2019**, *141* (5), 2054−2060.
(56) Alezi, D.; Spanopoulos, I.; Tsangarakis, C.; Shkurenko, A.; Adil, K.; Belmabkhout, Y.; O'Keeffe, M.; Eddaoudi, M.; Trikalitis, P. N. Reticular Chemistry at Its Best: Directed Assembly of Hexagonal Building Units into the Awaited Metal-Organic Framework with the Intricate Polybenzene Topology, pbz-MOF. *J. Am. Chem. Soc.* **2016**, *138* (39), 12767−12770.
(57) Kumari, L.; Li, W. Z.; Xu, J. M.; Leblanc, R. M.; Wang, D. Z.; Li, Y.; Guo, H.; Zhang, J. Controlled Hydrothermal Synthesis of Zirconium Oxide Nanostructures and Their Optical Properties. *Cryst. Growth Des.* **2009**, *9* (9), 3874−3880.
(58) Morant, C.; Fernandez, A.; Gonzalezelipe, A. R.; Soriano, L.; Stampfl, A.; Bradshaw, A. M.; Sanz, J. M. Electronic-Structure of Stoichiometric and Ar+-Bombarded Zro2 Determined by Resonant Photoemission. *Phys. Rev. B* **1995**, *52* (16), 11711−11720.
(59) Suginome, S.; Sato, H.; Hori, A.; Mishima, A.; Harada, Y.; Kusaka, S.; Matsuda, R.; Pirillo, J.; Hijikata, Y.; Aida, T. One-Step Synthesis of an Adaptive Nanographene MOF: Adsorbed Gas-Dependent Geometrical Diversity. *J. Am. Chem. Soc.* **2019**, *141* (39), 15649−15655.
(60) Baier, D. M.; Gratz, S.; Jahromi, B. F.; Hellmann, S.; Bergheim, K.; Pickhardt, W.; Schmid, R.; Borchardt, L. Beyond the Scholl reaction - one-step planarization and edge chlorination of nanographenes by mechanochemistry. *RSC Adv.* **2021**, *11* (60), 38026−38032.
(61) Loos, M.; Gerber, C.; Corona, F.; Hollender, J.; Singer, H. Accelerated Isotope Fine Structure Calculation Using Pruned Transition Trees. *Anal. Chem.* **2015**, *87* (11), 5738−5744.
(62) Rathore, R.; Burns, C. L. A practical one-pot synthesis of soluble hexa-peri-hexabenzocoronene and isolation of its cation-radical salt. *J. Org. Chem.* **2003**, *68* (10), 4071−4074.
(63) Rathore, R.; Kumar, A. S.; Lindeman, S. V.; Kochi, J. K. Preparation and structures of crystalline aromatic cation-radical salts. Triethyloxonium hexachloroantimonate as a novel (one-electron) oxidant. *J. Org. Chem.* **1998**, *63* (17), 5847−5856.
(64) Rathore, R.; Kochi, J. K. Isolation of Novel Radical Cations from Hydroquinone Ethers - Conformational Transition of the Methoxy Group Upon Electron-Transfer. *J. Org. Chem.* **1995**, *60* (14), 4399−4411.
(65) Hu, Y.; Wang, D.; Baumgarten, M.; Schollmeyer, D.; Müllen, K.; Narita, A. Spiro- fused bis- hexa- peri- hexabenzocoronene. *Chem. Commun.* **2018**, *54* (96), 13575−13578.
(66) Horibe, T.; Ohmura, S.; Ishihara, K. Structure and Reactivity of Aromatic Radical Cations Generated by FeCl3. *J. Am. Chem. Soc.* **2019**, *141* (5), 1877−1881.
(67) Zheng, X.; Drummer, M. C.; He, H. Y.; Rayder, T. M.; Niklas, J.; Weingartz, N. P.; Bolotin, I. L.; Singh, V.; Kramar, B. V.; Chen, L. X.; Hupp, J. T.; Poluektov, O. G.; Farha, O. K.; Zapol, P.; Glusac, K. D. Photoreactive Carbon Dioxide Capture by a Zirconium-Nanographene Metal-Organic Framework. *J. Phys. Chem. Lett.* **2023**, *14*, 4334−4341.
(68) Wang, Q.; Domen, K. Particulate Photocatalysts for Light-Driven Water Splitting: Mechanisms, Challenges, and Design Strategies. *Chem. Rev.* **2020**, *120* (2), 919−985.
(69) Zhan, W.; Gao, H.; Yang, Y.; Li, X.; Zhu, Q.-L. Rational Design of Metal-Organic Framework-Based Materials for Photocatalytic CO2 Reduction. *Adv. Energy Sustainability Res.* **2022**, *3* (7), No. 2200004.
(70) Shi, Y.; Yang, A. F.; Cao, C. S.; Zhao, B. Applications of MOFs: Recent advances in photocatalytic hydrogen production from water. *Coord. Chem. Rev.* **2019**, *390*, 50−75.

https://doi.org/10.1021/acsaom.3c00220
ACS Appl. Opt. Mater. 2023, 1, 1643−1650